Contemporary Mathematics
https://ojs.wiserpub.com/index.php/CM/

Research Article

A Mathematical Study of Rectangular and Triangular Fins with Variable Thermal Conductivity Through Local Thermal Equilibrium and Local Thermal Non-Equilibrium Fluid Models by Means of Artificial Neural Network

Manaswini R.[1], S. Manjunatha[1], Khalil Ur Rehman[2*], Tanuja T. N.[3], Wasfi Shatanawi[2]

[1] Department of Mathematics, CHRIST (Deemed to be University), Bengaluru, Karnataka 560076, India
[2] Department of Mathematics and Sciences, College of Science and Humanities, Prince Sultan University, Riyadh 11586, Saudi Arabia
[3] Department of Mathematics, Amity School of Applied Sciences, Amity University, Bengaluru, Karnataka 562110, India
E-mail: kurrehman@psu.edu.sa

Received: 20 October 2025; **Revised:** 9 December 2025; **Accepted:** 30 January 2026

Abstract: A mathematical approach is employed to examine the heat transmission capabilities of rectangular and triangular porous fins in both Local Thermal Equilibrium (LTE) and Local Thermal Non-Equilibrium (LTNE) scenarios. To provide a more accurate depiction of the thermal interaction between the solid and fluid phases, the LTNE model uses two coupled energy equations to represent their respective temperature fields. In contrast, the LTE model is controlled by a single energy equation and assumes a constant temperature throughout the phases. In order to ascertain the temperature distribution and overall thermal performance of the fin system, the governing equations are developed using the basic concepts of heat conduction and convection. To achieve enhanced heat transmission ability and greater thermal conductivity, the fluid phase is blended with Ag, Au, and TiO_2 as nanoparticles. These formulated equations have been turned into dimensionless nonlinear ordinary differential equations, and then Runge-Kutta Fehlberg fourth-fifth order (RKF-45) approach is adopted to solve them numerically. The credibility and accuracy of the results are ensured by benchmarking with previously established findings. The influence of important parameters on the thermal behavior of porous fins is visually examined by graphical analysis. Additionally, an Artificial Neural Network (ANN) method is employed to precisely evaluate and forecast the rate of heat transmission. It attains a high regression coefficient $R = 1$, indicating that the predictions are highly reliable. The analysis shows that the Nusselt number for the LTNE model is about 26.19% higher than that of the LTE model, indicating enhanced heat transfer performance.

***Keywords*:** Local Thermal Equilibrium (LTE), Local Thermal Non-Equilibrium (LTNE), thermal analysis, triangular/rectangular fins, ternary nanofluid, artificial neural network

MSC: 80A19, 80M20, 65L06

Nomenclature

a_{sf}	Interfacial area per unit volume of porous fin (m^{-1})	$a_{sf} = \frac{A_{sf}}{Wt_b\Delta x}$

Copyright ©2026 Khalil Ur Rehman, et al.
DOI: https://doi.org/10.37256/cm.7320268950
This is an open-access article distributed under a CC BY license
(Creative Commons Attribution 4.0 International License)
https://creativecommons.org/licenses/by/4.0/

A_{sf}	Interfacial area between nanofluid and solid phases (m^2)
g	Acceleration due to gravity (ms^{-2})
x	Axial coordinates (m)
X	Non-dimensional coordinate
h_{sf}	Convective heat transfer coefficient between solid and fluid phase
$A_b^* = Wt$	Cross section area of the fin (m^{-2})
h_L	External convective heat transfer coefficient $Wm^{-2}K^{-1}$
h_a	Convective coefficient of mass transfer $kgm^{-2}s^{-1}$
p	Perimeter of cross section (m)
q^*	Heat flux
q_x^*	Conductive heat transfer flux along x (Wm^2)
L	Length (m)
W	Width (m)
M^*	Mass flow rate (kgs^{-1})
K	Permeability (m^2)
C_p	Specific heat capacitance ($Jkg^{-1}K^{-1}$)
Bi	Biot number, $Bi = \dfrac{a_{sf}h_{sf}L^2}{(1-\varphi)k_a} = \dfrac{h_{sf}a_{sf}L^2}{\varphi K_a}$
R	Radiation conduction parameter, $R = \dfrac{4\sigma T_\infty^3}{3\beta_R(1-\varphi)k_f} = \dfrac{4\sigma T_\infty^3}{3\beta_R \phi k_f}$
Ra	Rayleigh number, $Ra = \dfrac{(\rho C_p)_{tnf} gk(\rho\beta)_{tnf} t_b (T_b{}^* - T_\infty^*)}{\varphi K_a \mu_{tnf}}$
H	Hartmann number, $H = \dfrac{\sigma_{tnf} B_0^2 u^2 L^2}{\varphi K_a W \cdot t_b}$
m_2	Wet porous parameter, $m_2 = Bik + m_1$
m_1	$m_1 = \dfrac{L^2 H_{sf} i_{fg} a_{sf} b_2}{Le^{2/3} (C_p)_f K_a (1-\varphi)}$
h_a	Convective coefficient of mass transfer ($kg\ m^{-2}s^{-1}$)
F_{f-a}	Shape factor for radiation heat transfer
tnf	Ternary hybrid nanofluid
i_{fg}	Latent heat of evaporation (Jkg^{-1})
b	Base of fin
m	Mass transfer (kgs^{-1})
$w_s - w_f = b_2(T_s^* - T_f^*)$	Humidity ratio

Greek symbols

β_R	Rosseland means extinction coefficient (m)
θ	Dimensionless temperature
Ω	Dimensionless thermal conductivity parameter
μ	Dynamic viscosity ($kgm^{-1}s^{-1}$)
ρ	Density (kgm^{-3})
χ	External convective parameter $\chi = \dfrac{Lh_L}{K_a}$
σ	Stefan-Boltzmann constant (Wm)
v_w	Velocity (ms^{-1})
φ	Porosity

τ Thickness (m)
ε^* Emissivity coefficient
γ Porosity, $\gamma = \dfrac{(1-\varphi)}{\varphi}$

1. Introduction

Extended surfaces, also referred as fin, are essential in numerous engineering applications such as chemical processing equipment, automotive systems, refrigeration, and air conditioning. Fin is primarily used to enhance heat transmission either by radiation, convection or the combination of both between the supporting surface and the surrounding environment. Fin functions effectively when placed on the side of a wall with the highest thermal resistance, since they boost surface conductivity by spreading the effective heat transmission area. Due to the fin's superior heat dissipation mechanism makes it extremely important for many industrial applications. For instance, fins are incorporated into the engine cylinder of air-cooled internal combustion engines to control temperature. By expanding the surface area subjected to airflow, these fins assist in avoiding overheating by facilitating more efficient heat dissipation through convection. Harper and Brown [1] carried out the first quantitative study of the complex relationship between convection and conduction along an extended surface. Güvenç and Yüncü [2] examines natural convection heat transmission in fin arrays on a vertical basis experimentally. Study discovered that the performance of fin is greatly influenced by the ideal spacing between them. Furthermore, numerous applications of fin in engineering and energy systems have sparked a growing interest among researchers in exploring the impact of various fin geometries. The thermal efficiency of solar air heaters with and without longitudinal fins is experimentally compared by Chabane et al. [3]. The thermal behavior of an internal heat-generating convective-radiative concave fin was investigated by Varun et al. [4]. Additionally, introducing porosity to fin improves thermal performance by increasing surface area and airflow, which facilitates heat transfer effectively. Kiwan and Al-Nimr [5] investigated the advantages of porous fins over solid fins in terms of heat transmission. Conclusions of the study show how porosity improves the performance while utilizing less material. By employing Darcy's model and energy balance, Saedodin and Sadeghi [6] examine long porous and solid fins in natural convection. Ahmadpour et al. [7] observed that radial fins improve heat transfer and shorten freezing time in an annular cylinder used for latent heat storage. A moving fin with temperature-dependent thermal conductivity was examined by Han and Peng [8] in both convective and radiative conditions. Rostami and Ahmadi [9] highlighted the value of geometric design and the use of shape alteration to maximize thermal performance.

Over the years different fin geometries have been developed to optimize heat transfer efficiency for different applications. The thermal performance of the triangular and rectangular fins makes them stand out among other types of fins. Triangular fins are perfect for lightweight applications like aeronautical cooling and microelectronics because of their tapering design, which uses less material. In forced convection, their aerodynamic design also reduces air resistance. Rectangular fins are frequently found in power electronics, radiators, and industrial heat exchangers due to their consistent thickness, which allows for high heat transfer rates. Ullah et al. [10] examined the effectiveness of moving, permeable, and triangular fins in terms of heat transmission by studying several types of dimensionless characteristics. Saqib et al. [11] examined heat transport in moving radiative porous triangular systems. Ndlovu and Moitsheki [12] investigated the properties of heat flow in a vertically oriented porous rectangular fin using Darcy's model. Adhikari et al. [13] explored the induced convection of heat from straight rectangular fins at small Reynolds numbers. Shadlaghani et al. [14] studied the optimizing triangular fins for improved heat transmission in forced convection. Conclusion suggests that the triangular fins with a larger height-to-thickness ratio dissipated more heat and significantly improved thermal performance. Manni and Azzi [15] examined the effects of Reynolds number and fin spacing on air flow via a rectangular channel with spaced rectangular-triangular fins. Also, the efficiency of heat transport is greatly impacted by the fins varying thermal conductivity. Madhura et al. [16] investigated how radiation and magnetic fields affected heat transport in porous fins and found that efficiency significantly increased. Heat transfer in a moving triangular fin was examined by Roy et al. [17] highlighted the significance of convection parameters and temperature-dependent conductivity. Ananth et al. [18] investigated triangular

and rectangular fin shapes with internal heat generation and radiation. Chiu and Chen [19] studied the heat transfer in rectangular fins with variable thermal conductivity, highlighting its critical role in thermal management.

When compared to traditional cooling fluids, nanofluids which are created by distributing nanoparticles into a convectional fluid have noticeably better heat transfer capacities. Choi and Eastman [20] first proposed the idea of mono fluids in 1995. He showed how adding nanoparticles, such as copper oxide or aluminum oxide, to regular fluids might greatly improve their thermal characteristics. Enhancing convective heat transfer efficiency and increasing thermal conductivity were the main objectives of these nanofluids. Heat transmission is significantly enhanced by a curved rectangular fin in the presence of nanofluid, as demonstrated by Jalili et al. [21]. By incorporating the nanofluid, Khan et al. [22] explored the convective heat transmission in a triangular fin-shaped cavity. Since mono nanofluids have limits in heat transport and stability, hybrid nanofluids were developed by blending two nanoparticles for improved performance. Gireesha et al. [23] examined the thermal characteristics of a moving porous longitudinal fin submerged in a hybrid nanofluid with the impacts of thermal radiation and natural convection. Results demonstrated that fin with convective tips improve heat dissipation more efficiently than those with insulated tips. The heat transmission capabilities of triangular and rectangular fins coated with hybrid nanoparticles performing in both dry and wet environments were demonstrated by Raju et al. [24]. For the first time a theoretical study on combining three distinct nanoparticles in the base fluid referred to as a ternary hybrid nanofluid was demonstrated by Manjunath et al. [25]. Ouada et al. [26] investigated the heat transmission in a rectangular porous moving fin by using a ternary hybrid nanofluid of various shapes. Hence, ternary nanofluids are utilized in various industries, including heat exchangers, automotive cooling, and electronics [27–30].

In high-performance applications, the design of complex heat management systems depends heavily on the ideas of Local Thermal Equilibrium (LTE) and Local Thermal Non-Equilibrium (LTNE). LTE makes the assumption that effective heat transport causes the temperature of the phases to quickly attain equilibrium. Hoseinzadeh et al. [31] investigated the transmission of heat in a permeable rectangular fin utilizing LTE assumptions. Jeng et al. [32] employed an algorithmic model that reliably forecasts heat transmission performance in a variety of porous media to investigate heat transfer in porous rectangular fins under the LTE assumption. Jaiswal et al. [33] examined the importance of the triangular fin in order to improve heat transmission in the presence of ternary nanofluid. On the other hand, LTNE occurs when various components fail to achieve thermal equilibrium, which means that temperature differentials between them last longer. It is clear from Manaswini et al. [34] study that the LTNE model more accurately depicts the behavior of heat transfer than the LTE model, where there is a temperature differential between the solid and fluid phases. Thimlapura Nagaraju et al. [35] utilized the LTNE model to investigate the transmission of heat in a wetted porous rectangular fin. Their research examines the effects of utilizing a ternary hybrid nanofluid on thermal conductivity and heat transfer efficiency. Manjunatha et al. [36] investigates heat transfer in a rectangular porous fin under LTNE conditions with ternary ferrofluid by considering the effects of radiation, magnetic fields. Buonomo et al. [37] investigated the movement of heat in a porous rectangular fin employing the LTNE model, taking radiation and natural convection into consideration. The results suggest that temperature changes between the solid and fluid phases, with important variables like Biot and Rayleigh numbers influencing heat transmission behavior.

It is evident from the above literature analysis that, heat transfer optimization requires an exact balance between fluid composition, modeling, and the geometry. So, the rectangular fins are often preferred for their uniform temperature distribution and effective heat dissipation. However, triangular fins also play a role in heat transmission characteristics due to their tapering shape. The proper modeling technique is necessary to forecast their thermal behavior with accuracy. While the LTNE model captures temperature changes within the system, the LTE model simplifies analysis by assuming thermal equilibrium. Thus, the analysis of rectangular and triangular fins with varying thermal conductivity under LTE and LTNE conditions is the focus of this work. In order to accomplish this, the RKF45 method is used to solve the governing equations numerically, ensuring precise analysis of the temperature distribution and overall performance of heat transfer. Further, to improve heat transfer, stability, and conductivity, Ag, Au, and TiO_2 are blended with water to create a ternary nanofluid. Since Ag has a high thermal conductivity and ensures quick transfer of heat, it is given the first priority. Following this, Au is added to improve nanoparticle dispersion and fluid stability. Finally, TiO_2 is incorporated to enhance heat absorption and stability of the system, making this extremely effective. Additionally, Artificial Neural Networks (ANNs) are utilized to predict accuracy, allowing for more dependable analysis and optimization of the thermal behavior in intricate systems.

This study has significance in applications like energy storage, electronic cooling, and high-performance heat exchangers, where effective thermal management is essential.

2. Mathematical model

This study compares heat transfer capabilities of a porous rectangular and triangular fin under LTE and LTNE models. Each fin has specific length L and the area of cross section is $W * t(X)$ which is defined by its constant width W and thickness $t(X)$ as illustrated in Figure 1a, b. Heat transport along the fin's length is the primary focus of the investigation. Fin exterior surface acts as a way for thermal energy by transferring heat from a heated base temperature T_b that is maintained at a constant temperature into the surrounding T_∞. In addition to the aforementioned geometric structure, the analysis is carried out under the following presumptions.

• It is assumed that the temperature profile varies only along its length and radial or transverse variations are neglected.

• Both LTE and LTNE approaches are employed to investigate the porous fin using a steady-state, one-dimensional heat transfer system. Where the temperature distribution is assumed not to change with time, as the fin has reached thermal equilibrium with its surroundings.

• An accurate heat dissipation analysis is carried out by integration of the convective contributions from fluid movement and surface thermal losses.

• With the goal to capture both convective and radiative heat transfer effects, the fin surface is treated with a ternary nanofluid that contains Ag, Au, and TiO_2 nanoparticles distributed in a convectional fluid H_2O.

• The interaction between the solid matrix and fluid flow within the fin porous structure.

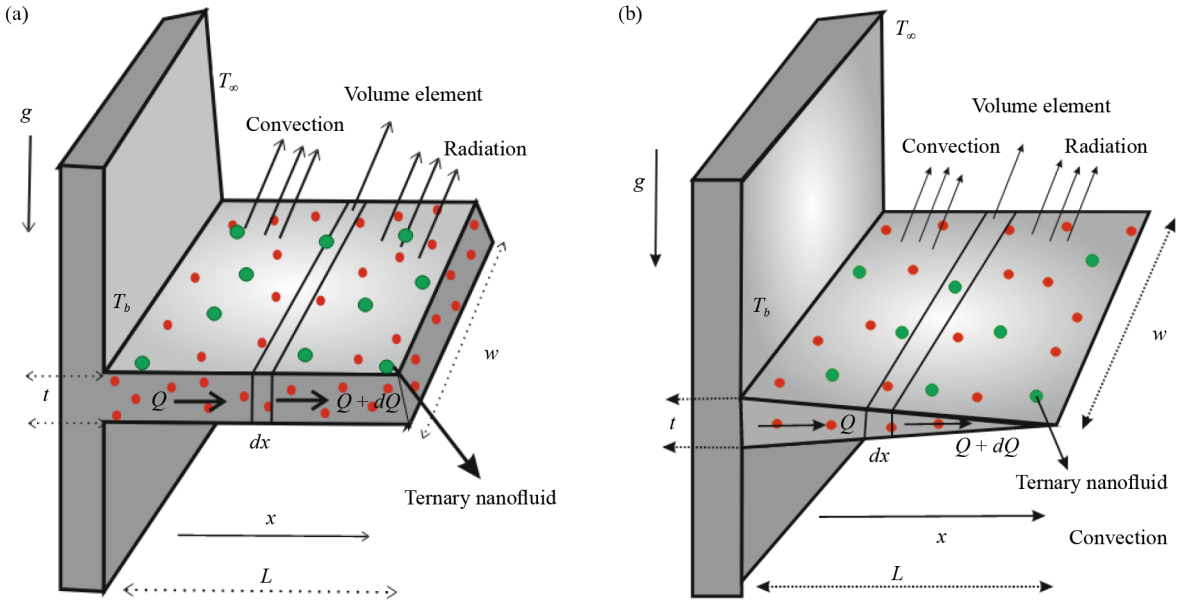


Figure 1. (a) Rectangular profile and (b) Triangular profile

With consideration of all the aforementioned hypotheses, equation (1)–(3) represents the fin's balanced energy equation.

LTE model:

$$A_q\left[q^*(x)-q^*(x+\Delta x)\right]=M^*C_{ptnf}\left(T^*-T_\infty^*\right)+h_LP\Delta x(1-\varphi)\left(T^*-T_\infty^*\right)+\frac{J_C\times J_C}{\sigma}\left(T^*-T_\infty^*\right)\Delta x$$

$$+P\Delta x\sigma_{st}\varsigma\left(T^{*4}-T_\infty^{*4}\right)+h_{sf}A_{sf}\left(T_s^*-T_f^*\right)+h_a i_{fg}A_{sf}\left(w_s^*-w_f^*\right). \tag{1}$$

LTNE Model:
Ternary Fluid Phase:

$$A_q\left[q^*(x)-q^*(x+\Delta x)\right]=M^*C_{ptnf}\left(T_f^*-T_\infty^*\right)+\frac{J_C\times J_C}{\sigma_{tnf}}\left(T^*-T_\infty^*\right)\Delta x+h_{sf}A_{sf}\left(T_s^*-T_f^*\right). \tag{2}$$

Solid Phase:

$$A_q\left[q^*(x)-q^*(x+\Delta x)\right]=h_LP\Delta x(1-\varphi)\left(T_s^*-T_\infty^*\right)+P\Delta x\sigma_{st}\varsigma\left(T^{*4}-T_\infty^{*4}\right)$$

$$+h_{sf}A_{sf}\left(T_s^*-T_f^*\right)+h_a i_{fg}A_{sf}\left(w_s^*-w_f^*\right)+\frac{J_C\times J_C}{\sigma_s}\left(T^*-T_\infty^*\right)\Delta x. \tag{3}$$

The mathematical equation for the impact of buoyancy force on fluid mass flow rate through a porous media is as outlined below:

$$M^*=\rho_{tnf}(W\cdot\Delta x)v_w, \tag{4}$$

here, v_w represents the fluid velocity inside the porous material that is driven by buoyancy. The interaction between the fluid and the porous structure is described using the Darcy model.

$$v_w=\frac{gK(\rho\beta)_{tnf}}{\mu_{tnf}}\left(T^*-T_\infty^*\right)=\frac{gK(\rho\beta)_{tnf}}{\mu_{tnf}}\left(T_f{}^*-T_\infty^*\right). \tag{5}$$

The energy flux vector at the fin's base that takes radiation and conduction into consideration is described below:

$$q^*=q^*(x)+q^*(x+\Delta x). \tag{6}$$

The following is the expression for the $q^*(x)$ and $q^*(x+\Delta x)$ obtained by using Fourier's rule of conduction and Rosseland approximation respectively:

$$q^*(x)=K^*(T)\frac{dT^*}{dx}\quad\text{and}\quad q^*(x+\Delta x)=-\frac{4\sigma_{st}A_c}{3\beta_R}\frac{dT^{*4}}{dx}, \tag{7}$$

where $K^*(T)=K_a\left[1+\lambda\left(T-T_\infty\right)\right]=K_a\left[1+\lambda\left(T_s-T_\infty\right)\right]=K_a\left[1+\lambda\left(T_f-T_\infty\right)\right]$ is the variable thermal conductivity.

The term T^{*4} can be employed when the temperature changes within the flow are thought to be relatively minimal.

$$T^{*4} \approx {T_\infty}^{*3}\left(4T^* - 3T_\infty^*\right). \tag{8}$$

Equations (4)–(5), and (7)–(8) are substituted into equations (1)–(3), then the resulting equations as follows:
LTE model:

$$\begin{aligned}\frac{d}{dx}X^n\left[(1-\varphi)K(T)\frac{dT^*}{dx} - \frac{4\sigma_{tnf}}{3\beta_R}\frac{dT^{*4}}{dx}\right] &= \frac{(\rho C_p)_{tnf}\, gk(\rho\beta)_{tnf}}{\mu_{tnf}t_b}\left(T^* - T_\infty^*\right)^2 \\ &+ \frac{h_L P(1-\varphi)}{Wt_b}\left(T^* - T_\infty^*\right) + \frac{\sigma_{tnf}B_0^2u^2}{t_bW\Delta x}\left(T^* - T_\infty^*\right) \\ &+ \frac{4P\Delta x\sigma_{st}F_{f-a}T_\infty^3}{Wt_b\Delta x}\left(T^{*4} - T_\infty^{*4}\right) + \frac{h_{sf}A_{sf}\left(T_s^* - T_f^*\right)}{Wt_b\Delta x} \\ &+ \frac{h_a i_{fg}A_{sf}\left(w_s^* - w_f^*\right)}{t_bW\Delta x}.\end{aligned} \tag{9}$$

LTNE model:

$$\varphi\frac{d}{dx}\left[X^nK(T)\frac{dT}{dx}\right] = \frac{(\rho C_p)_{tnf}\, gk(\rho\beta)_{tnf}}{t_b\mu_{tnf}}\left(T_f^* - T_\infty^*\right)^2 + \frac{\sigma_{tnf}B_0^2u^2\left(T_f^* - T_\infty^*\right)}{t_b} + \frac{h_{sf}A_{sf}\left(T_s^* - T_f^*\right)}{W\cdot t_b\Delta x}. \tag{10}$$

$$\begin{aligned}\left[(1-\varphi)\frac{d}{dx}\left(X^nK(T)\frac{dT_s^*}{dx}\right) + \frac{16\sigma T_\infty^3}{3\beta_R}\frac{d}{dx}\frac{dT_s^*}{dx}\right] &= \frac{h_L P\Delta x(1-\varphi)}{Wt_b\Delta x}\left(T_s^* - T_\infty^*\right) \\ &+ \frac{4P\Delta x\sigma_{st}F_{f-a}T_\infty^3}{Wt_b\Delta x}\left(T_s^* - T_\infty^*\right) + \frac{h_{sf}A_{sf}}{Wt_b\Delta x}\left(T_s^* - T_f^*\right) \\ &+ \frac{h_a i_{fg}A_{sf}}{Wt_b\Delta x}\left(w_s^* - w_f^*\right) + \frac{\sigma_{tnf}B^2u^2}{Wt_b\Delta x}\left(T^* - T_\infty^*\right)\Delta x,\end{aligned} \tag{11}$$

where, $h_{sf} = h_a\left(C_p\right)_f Le^{2/3}$.

Boundary conditions are:

The insulated tip boundary condition for the study is shown as follows. It is assumed that the fin tip is adiabatic, which means that no heat is transferred from the tip to the environment. All heat transported from the fin is dissipated through its lateral surfaces because there is no physical heat flux at the tip. This condition is frequently applied to thin fins that are utilized in heat exchangers or electronics cooling, when tip losses are minimal.

$$T^*(x) = T_f^*(x) = T_s^*(x) = T_b \quad \text{at} \quad x = 0$$

$$\frac{dT^*}{dx} = \frac{dT_f^*}{dx} = \frac{dT_s^*}{dx} = 0 \quad \text{at} \quad x = L. \tag{12}$$

Below is the description of the dimensionless parameters:

$$\theta = \frac{T^* - T_\infty^*}{T_b^* - T_\infty^*}, \quad \theta_f = \frac{T_f^* - T_\infty^*}{T_b^* - T_\infty^*}, \quad \theta_s = \frac{T_s^* - T_\infty^*}{T_b^* - T_\infty^*}, \quad X = \frac{x}{L}, \quad \tau = \frac{t_b}{L}. \tag{13}$$

The thermophysical properties of Ag, Au, and TiO_2 with base fluid are presented in Table 1 and their associated characteristics are demonstrated in the Table 2.

Table 1. Thermophysical properties of Ag, Au, TiO_2, and H_2O

Properties	Ag	Au	TiO_2	H_2O
ρ (kg/m^3)	10,500	19,300	4,250	997.1
k (W/m·K)	429	318	8.9538	0.6071
σ (S/m)	6.3×10^7	4.1×10^7	2.6×10^6	0.05
C_p (J/kg·K)	235	129	686.2	4,179

Table 2. Thermophysical model of ternary nanofluid

Properties	Hybrid nanofluid
Density	$\rho_{tnf} = (1-\phi_1)\left\{(1-\phi_2)\left[(1-\phi_3)\rho_f + \phi_3\rho_3\right] + \phi_2\rho_2\right\} + \phi_1\rho_1$
Heat capacity	$(\rho C_p)_{hnf} = (1-\phi_3)\left[(1-\phi_2)\left\{(1-\phi_1) + \phi_1 (\rho C_p)_1\right\} + \phi_2 (\rho C_p)_2\right] + \phi_3 (\rho C_p)_3$
Viscosity	$\mu_{tnf} = \frac{\mu_f}{(1-\phi_1)^{2.5}(1-\phi_2)^{2.5}(1-\phi_3)^{2.5}}$
Thermal conductivity	$\frac{k_{tnf}}{k_{hnf}} = \frac{k_1 + 2k_{tnf} - 2\phi_1\left(k_{tnf} - k_1\right)}{k_1 + 2k_{tnf} + \phi_1\left(k_{hnf} - k_1\right)}$, where $\frac{k_{hnf}}{k_{nf}} = \frac{k_2 + 2k_{nf} - 2\phi_2(k_{nf} - k_2)}{k_2 + 2k_{nf} + \phi_2(k_{nf} - k_2)}$, $\frac{k_{nf}}{k_f} = \frac{k_3 + 2k_f - 2\phi_3\left(k_f - k_3\right)}{k_3 + 2k_f + \phi_3\left(k_f - k_3\right)}$
Electrical conductivity	$\frac{\sigma_{tnf}}{\sigma_{hnf}} = \frac{(1+2\phi_1)\sigma_1 + (1-2\phi_1)\sigma_{hnf}}{(1-\phi_1)\sigma_1 + (1+\phi_1)\sigma_{hnf}}$, where $\frac{\sigma_{hnf}}{\sigma_{nf}} = \frac{(1+2\phi_2)\sigma_2 + (1-2\phi_2)\sigma_{nf}}{(1-\phi_2)\sigma_2 + (1+\phi_2)\sigma_{nf}}$, $\frac{\sigma_{nf}}{\sigma_f} = \frac{(1+2\phi_3)\sigma_3 + (1-2\phi_3)\sigma_f}{(1-\phi_3)\sigma_3 + (1+\phi_3)\sigma_f}$

Equations (9)–(11) expressed as nondimensionalized equations by utilizing the previously defined nondimensional variables as in equation (13):

LTE model:

$$\left[X^n[1+\theta\Omega]\frac{d^2\theta}{dX^2}+\frac{d^2\theta}{dX^2}\Omega X^n+\frac{d\theta}{dX}[1+\Omega\theta]X^{n-1}n\right]+4R\left[X^n\frac{d^2\theta}{dX^2}+X^{n-1}n\frac{d\theta}{dX}\right]$$

$$=\frac{1}{A}\left[E\frac{Ra}{\tau^2}\theta+H\theta+(Rsa+\chi)\frac{2}{\tau}\theta+m_2\theta\right]. \tag{14}$$

LTNE model:
Fluid Phase:

$$\left[X^n\left[1+\theta_s\Lambda\right]\frac{d^2\theta_s}{dX^2}+\Lambda X^n\frac{d^2\theta_s}{dX^2}+\left[1+\theta_s\Lambda\right]X^{n-1}n\frac{d\theta_s}{dX}+4R\left[X^n\frac{d^2\theta_s}{dX^2}+X^{n-1}n\frac{d\theta_s}{dX}\right]\right]$$

$$=\frac{2}{\tau}(\chi+Rsa)\theta_s+m_2\left(\theta_s-\theta_f\right)+H\theta_s. \tag{15}$$

Solid Phase:

$$\left[X^n\left[1+\theta_s\Omega\right]\frac{d^2\theta}{dX^2}+\Omega X^n\frac{d^2\theta_s}{dX^2}+\left[1+\theta_s\Omega\right]X^{n-1}n\frac{d\theta_s}{dX}+4R\frac{d^2\theta_s}{dX^2}\right]=\frac{2}{\tau}(\chi+Rsa)\theta_s+m_2\left(\theta_s-\theta_f\right)+H\theta_s. \tag{16}$$

Nondimensionalized boundary conditions are:

$$\theta^*=\theta_f^*=\theta_s^*=1,\quad \text{at}\quad X=0,$$

$$\frac{d\theta^*}{dX}=\frac{d\theta_f^*}{dX}=\frac{d\theta_s^*}{dX}=0,\quad \text{at}\quad X=L. \tag{17}$$

The fundamental thermal behavior of the system is effectively understood by studying the derived quantities such as Nusselt number. Below are the Nusselt number obtained for the present study.

For LTE model:

$$Nu=\frac{q^*t}{k_{eq}(T_b-T_\infty)}=-\frac{(1-\varphi)kr}{\varphi+(1-\varphi)k}(1+4R)\theta'(0). \tag{18}$$

For LTNE model:

$$Nu_s=\frac{q_s^*t}{k_{eq}(T_b-T_\infty)}=-\frac{(1-\varphi)kr}{\varphi+(1-\varphi)k}(1+4R)\theta_s'(0). \tag{19}$$

$$Nu_f=\frac{q_f^*t}{k_{eq}(T_b-T_\infty)}=-\frac{(1-\varphi)\tau}{\varphi+(1-\varphi)k}\theta_f'(0). \tag{20}$$

Equations (19) and (20) are added to determine the rectangular permeable fin's overall Nusselt number for LTNE model:

$$Nu = Nu_s + Nu_f. \tag{21}$$

Where, $k_{eq} = \varphi k_f + (1-\varphi)k_s$.

3. Numerical analysis

An adaptive Runge-Kutta method known for its effective error control via dynamic step sizing and numerical stability is the RKF-45 method. It ensures dependable convergence even for complicated or nonlinear heat transfer equations by automatically modifying the step size to preserve accuracy by assessing faults at every level. At the beginning of the computation, the algorithm needs the initial conditions of the Ordinary Differential Equations (ODEs) and a chosen step size. The RKF-45 approach provides approximations of the ODE solutions at each stage and uses the differences between them to estimate the local inaccuracy. Until the solution achieves the intended goal, this iterative process is carried out. As a result, RKF-45 effectively solves the coupled non-linear differential equations in LTNE models and provides precise and reliable results. The following is a thorough explanation of the Runge-Kutta-Fehlberg numerical method for fourth and fifth order:

$$k_0 = f(x_i, y_i),$$

$$k_1 = f\left(x_i + \frac{1}{4}h, y_i + \frac{1}{4}hk_0\right),$$

$$k_2 = f\left(x_i + \frac{3}{8}h, y_i + \left(\frac{3}{32}k_0 + \frac{9}{32}k_1\right)h\right),$$

$$k_3 = f\left(x_i + \frac{12}{13}h, y_i + \left(\frac{1{,}932}{2{,}197}k_0 - \frac{7{,}200}{2{,}197}k_1 + \frac{7{,}296}{2{,}197}k_2\right)h\right),$$

$$k_4 = f\left(x_i + h, y_i + \left(\frac{439}{216}k_0 - 8k_1 + \frac{3{,}860}{513}k_2 - \frac{845}{4{,}104}k_3\right)h\right),$$

$$k_5 = f\left(x_i + \frac{1}{2}h, y_i + \left(-\frac{8}{27}k_0 + 2k_1 - \frac{3{,}544}{2{,}565}k_2 + \frac{1{,}859}{4{,}104}k_3 - \frac{11}{40}k_4\right)h\right),$$

$$y_{i+1} = y_i + \left(\frac{25}{216}k_0 + \frac{1{,}408}{2{,}565}k_2 + \frac{2{,}197}{4{,}104}k_3 - \frac{1}{5}k_4\right)h,$$

$$z_{i+1} = z_i + \left(\frac{16}{135}k_0 + \frac{6{,}656}{12{,}825}k_2 + \frac{28{,}561}{56{,}430}k_3 - \frac{9}{50}k_4 + \frac{2}{55}k_5\right)h.$$

In this method, the fourth- and fifth-order Runge-Kutta approximations are denoted by y and z, respectively. Their difference serves as an estimate of the local inaccuracy. If this inaccuracy is within the given tolerance, steps are accepted; if not, the calculation is repeated using a smaller step size, which is established as previously. The step size and convergence criterion used in this work are 10^{-6} and $\Delta\eta = 0.001$ respectively.

Mathematica is used to solve the ordinary differential equations numerically, yielding approximate solutions over the specified interval. The plot function is used to visualize the data, which are then tabulated at certain places for additional analysis.

4. Discussion of results

The thermal properties of ternary nanofluids in enhancing rate of heat transfer of fin with variable thermal conductivity are examined in this work. Particular attention is given to analyze the variations between LTE and LTNE models in rectangular and triangular fin profiles. The rosseland approximation is utilized to incorporate radiation and convection effects into the energy equation, while Darcy's law governs the fluid motion within the porous media. The governing equations are first converted into a dimensionless form then solved numerically using the RKF-45 technique. For both LTE and LTNE scenarios, model validation precisely demonstrates that it aligns with the prior research [25, 38] as shown in Tables 3 and 4.

Table 3. Validation for LTE model. Comparison for rectangular profile for $\theta(X)$ when $\beta = \phi_1 = \phi_2 = H = n = 0$, $R = Ra = 2$

X	0	0.2	0.4	0.6	0.8	1
Present study	1	0.844759	0.732097	0.655722	0.611473	0.59698
Ouada et al. [26]	1	0.846837	0.737237	0.659893	0.610784	0.592531

Table 4. Validation for LTNE model in the absence of nanofluid

	$\theta_{\text{fin-air}}$					
X	0	0.1	0.3	0.6	0.9	1
Present study	1	0.848159	0.603065	0.398447	0.310317	0.304651
Tanuja et al. [36]	1	0.84031	0.60206	0.39388	0.31087	0.30167

The impact of the H on the θ for both rectangular and triangular fins is shown in Figure 2a, b. The effect of a magnetic field on fluid motion is indicated by the Hartmann number, which represents the ratio of electromagnetic to viscous forces. Convective heat transmission is weakened by magnetic resistance, whereas heat conduction in the fin improves with increasing magnetic field strength, resulting in a decrease in temperature. Compared to the rectangular fin, the triangular fin exhibits lower temperatures because it releases heat more quickly due to its smaller surface area. While the LTE model permits faster dissipation and more efficient heat transmission, the LTNE model shows higher surface temperature as a sign of increased heat retention and decreased transfer efficiency. Typically, the Hartmann number H falls between 1 and 10, after which the magnetic field becomes extremely strong and excessively suppresses convection and fluid motion. Consequently, heat transfer declines and the fin functions essentially as a solid conductor with little convective influence.

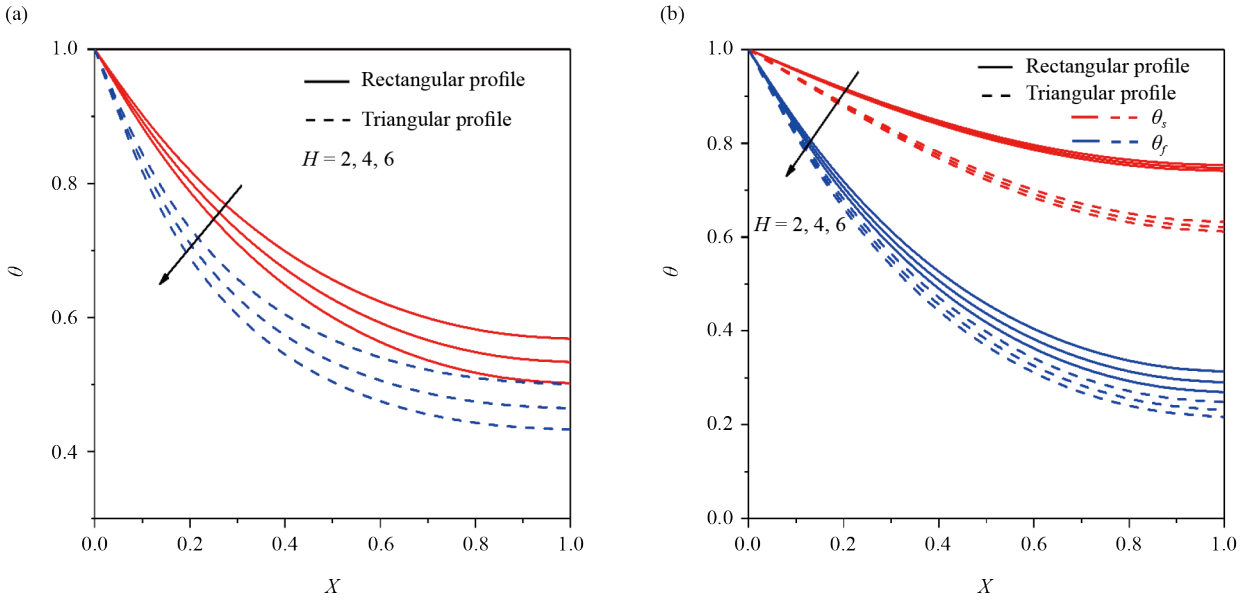


Figure 2. Effect of H on $\theta(X)$ for (a) LTE and (b) LTNE models

Figure 3a, b shows how the temperature distribution for the LTE and LTNE models is affected by Ω. As Ω increases, heat conduction improves due to a decrease in internal resistance within the fin. This enhances overall heat transfer and produces smoother, more consistent temperature profiles. From the Figure 3a it is observed that the enhancement in the LTE model results in a slow temperature rise and effective heat spreading. But the θ_s and θ_f react differently in the LTNE model by producing minute temperature fluctuations that represent a more realistic thermal behavior as observed by Figure 3b. This is demonstrated practically in heat sinks, where copper or aluminum conduct heat more uniformly than steel. The fin achieves maximum conduction efficiency when the Ω is increased beyond a certain point, and any additional increase results in minimal thermal improvement, hence normally Ω ranges from 1 to 10.

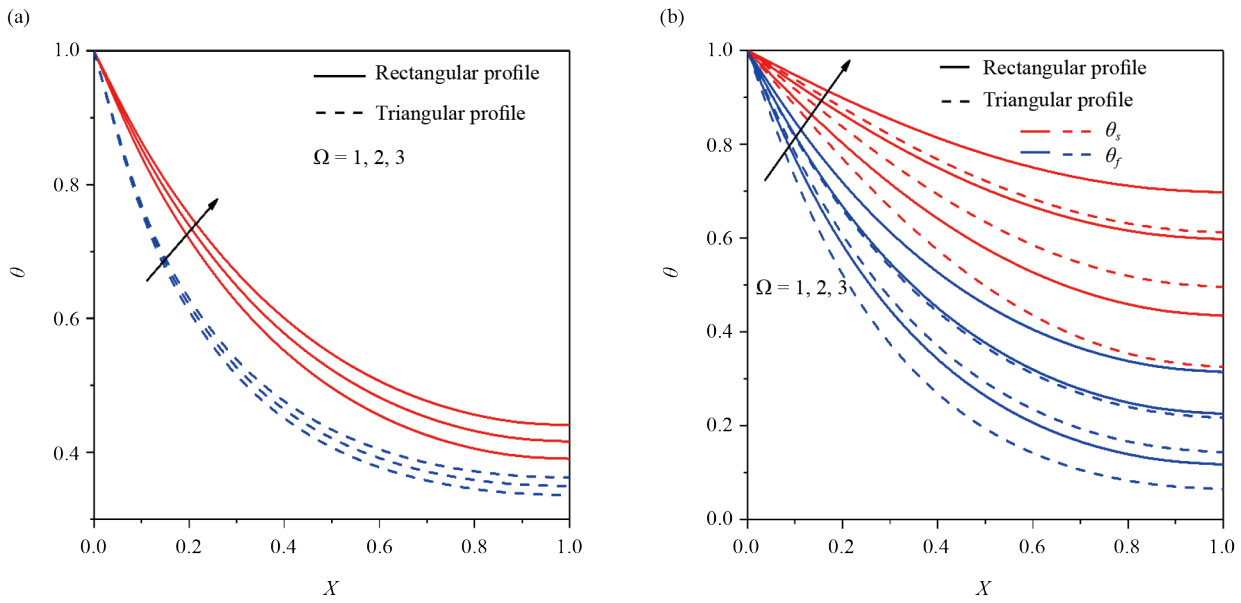


Figure 3. Effect of Ω on $\theta(X)$ for (a) LTE and (b) LTNE models

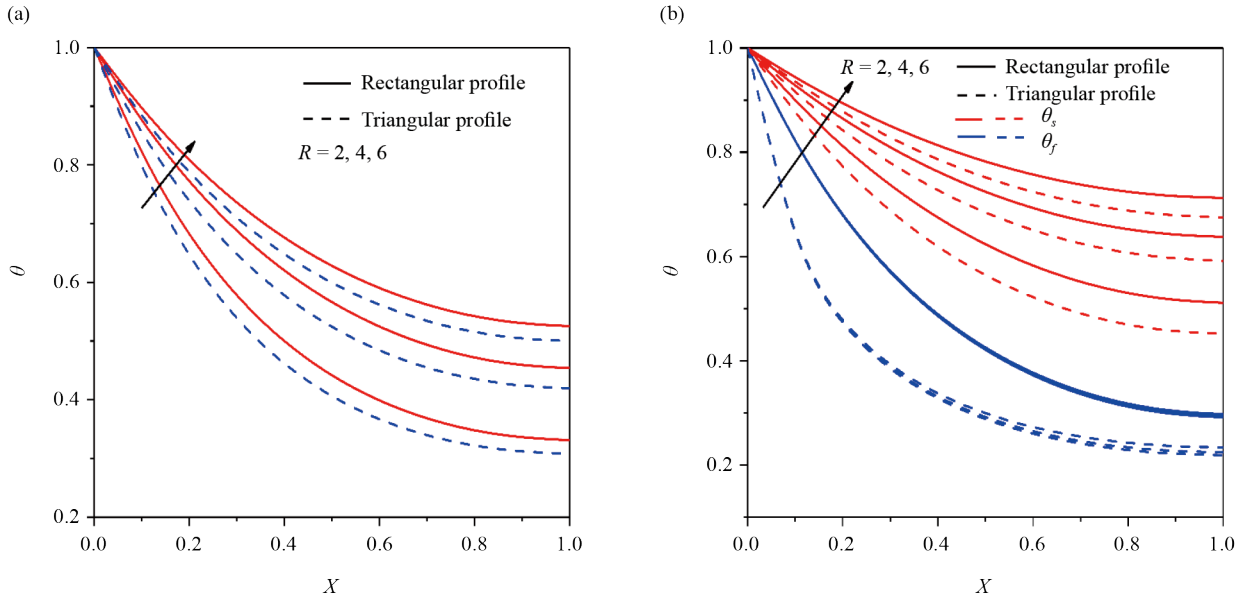


Figure 4. Effect of R on $\theta(X)$ for (a) LTE and (b) LTNE models

As shown in Figure 4a, b, the temperature distribution in both LTE and LTNE models changes noticeably with variations in the parameter R. Radiative heat flux strengthens with growing R, trapping more heat and rising the fin temperature. In Figure 4a the temperature climbs steadily with R in the LTE model, indicating consistent radiative heating. The solid and fluid phases in the LTNE model absorb radiative radiation at varying rates, which results in a little temperature differential between them as shown in Figure 4b. This version provides a more realistic image of radiative heat transport within the fin by highlighting the unequal effects of radiation on each phase. Solar panels and furnace walls provide a real-world example, as increased radiation raises the surface temperature. In order to ensure stability and realistic, R usually falls between 0.01 and 10 in laminar flow.

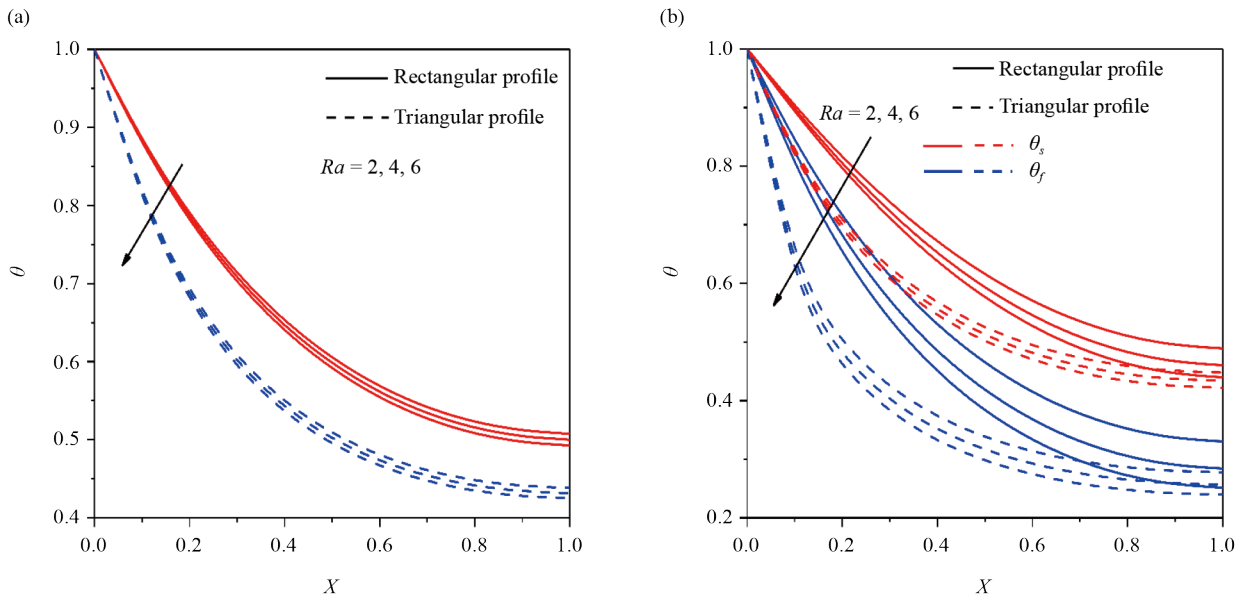


Figure 5. Effect of Ra on $\theta(X)$ for (a) LTE and (b) LTNE models

A fin's size, fluid characteristics, and temperature differential with its surroundings are some of the parameters that are considered when determining the *Ra*. In order to depict a conduct-dominated environment and ensure stable, laminar heat transfer within the fin, a low range of $0 \leq Ra \leq 100$ is employed in this study. Figure 5a, b describes how the strength of buoyancy-driven convection is indicated by the Rayleigh number in heat transmission. As a result of the greater temperature differential between the fin surface and the surrounding fluid, buoyancy forces increase as *Ra* rises. Increased heat removal from the fin surface and a corresponding drop in temperature result from this enhancement of natural convection, in which the warmer fluid rises and is replaced by the cooler one. Higher *Ra* encourages better heat dissipation and stronger convection in the LTE model as shown in Figure 5a, where the triangular fin displays lower temperatures than the rectangular one.

The degree of radiative heat exchange between the fin surface and its surroundings is shown by *Rsa* (Figure 6). The fin surface emits more thermal energy when *Rsa* rises because the radiation becomes more dominant than conduction. The overall fin temperature rises as a result of improved radiative feedback. While minor temperature variations arise in the LTNE model as a result of unequal radiative absorption between the phases, a greater *Rsa* in the LTE model results in a smoother and more consistent temperature profile. For stable laminar flow, *Rsa* typically falls between 0 and 10, beyond this threshold, conduction is outweighed by radiation, resulting in numerical instability and an irrational temperature increase.

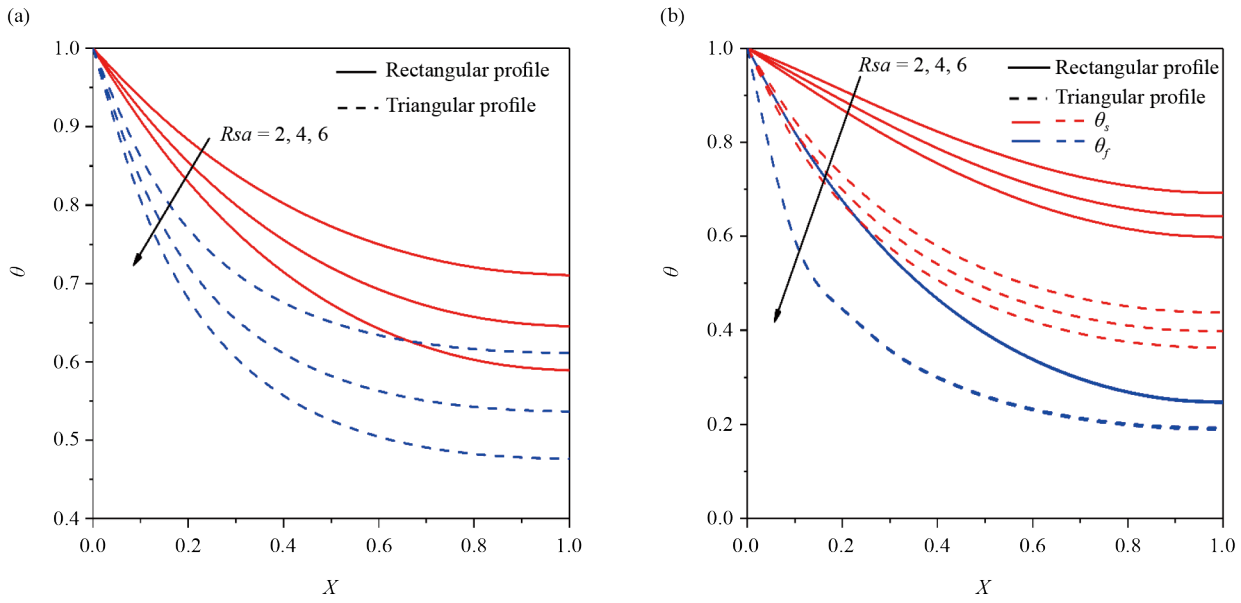


Figure 6. Effect of *Rsa* on $\theta(X)$ for (a) LTE and (b) LTNE models

An important factor in heat conduction is the thickness parameter τ, which is the ratio of the fin's thickness to its characteristic length. A thicker fin with a greater area improves heat conduction close to the base as τ rises. But too much thickness raises thermal resistance, which lowers heat transmission to the tip and raises the surface temperature a little. While there are slight variations between the solid and fluid phases in the LTNE model, temperature change in the LTE model is uniform and smooth. The parameter is varied between 0 and 2 to capture both thin and moderately a thick fin. Rectangular fins with higher surface area dissipate heat more effectively, whereas triangular fin tapering design causes an even temperature rise throughout their length, as observed in Figure 7a, b.

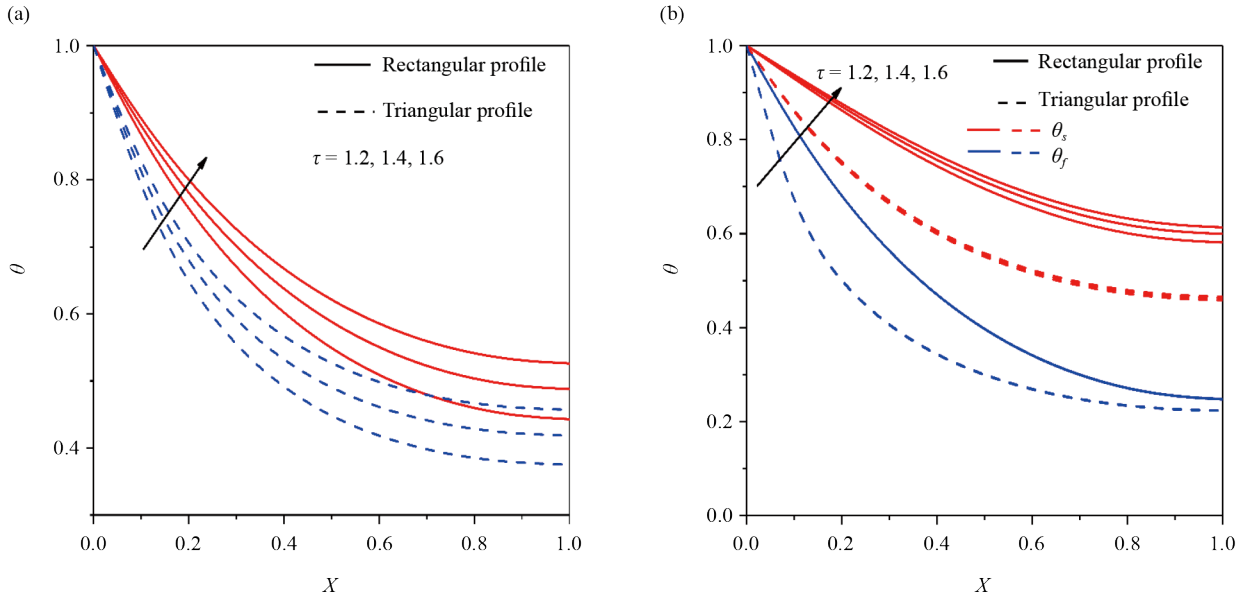


Figure 7. Effect of τ on $\theta(X)$ for (a) LTE and (b) LTNE models

Considering Figure 8a, b, the efficiency of heat removal to the surrounding fluid is determined by the external convective parameter χ, which is the ratio of convective to conductive heat transfer at the fin surface. A reduced temperature distribution over the fin length is the result of elevated convection, which improves heat loss from the fin surface as χ rises. The higher χ results in a smoother thermal gradient and faster heat removal in the LTE model, but uneven heat exchange in the LTNE model makes the temperature difference between the solid and fluid phases appear to be greater. This parameter is essential for studying fins in situations with significant cooling or forced convection. To investigate its impact on fin temperature distribution and guarantee steady and physically accurate convective behavior, the χ is adjusted in this study between 0.0001 and 1.0.

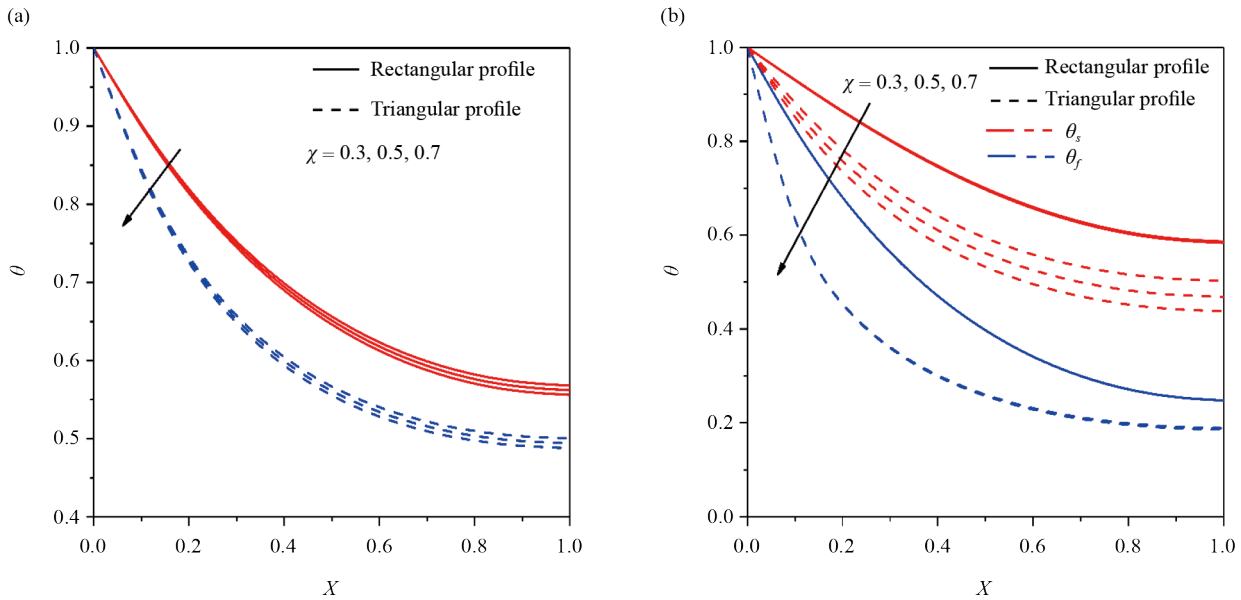


Figure 8. Effect of χ on $\theta(X)$ for (a) LTE and (b) LTNE models

The concentration of nanoparticles in the base fluid is represented by the solid volume fraction ϕ, which has a major impact on the fin's thermal performance. Heat transfer is improved and the temperature gradient along the fin is decreased when ϕ rises, which is due to the nanofluid's improved effective thermal conductivity (see Figure 9a, b). Uneven heat exchange between the solid and fluid phases causes minor changes in the LTNE model, whereas the LTE model shows smoother temperature profiles as ϕ rises. The ϕ is usually considered up to 3%–4% to preserve physical stability and prevent particle agglomeration, since going over this range might result in sedimentation of nanoparticles.

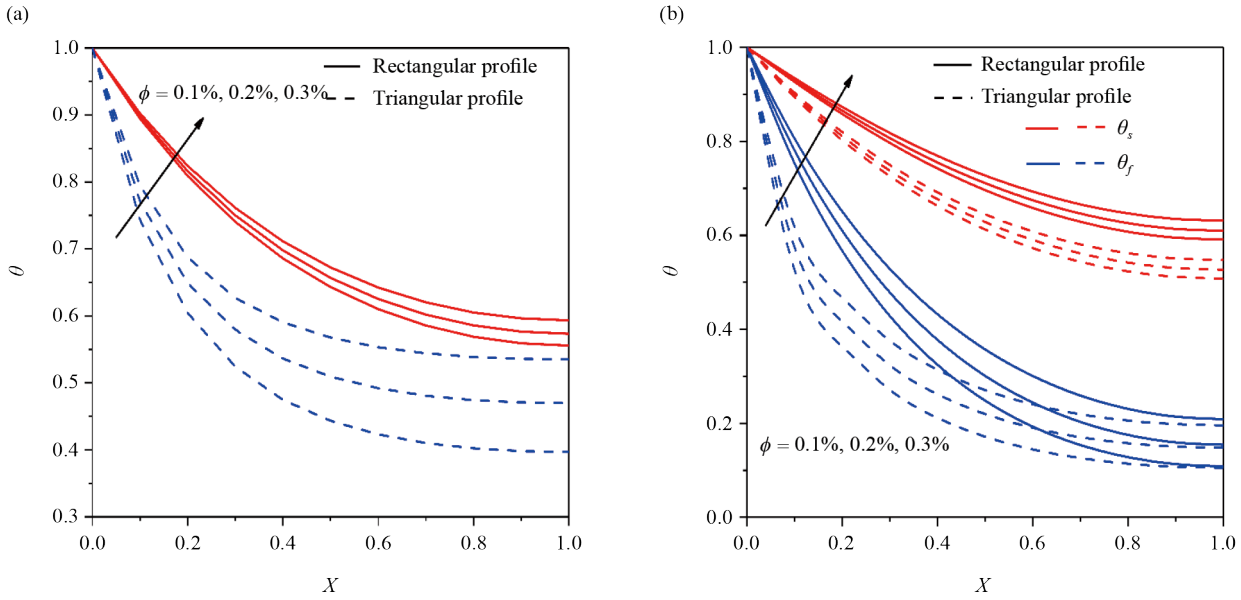


Figure 9. Effect of ϕ on $\theta(X)$ for (a) LTE and (b) LTNE models

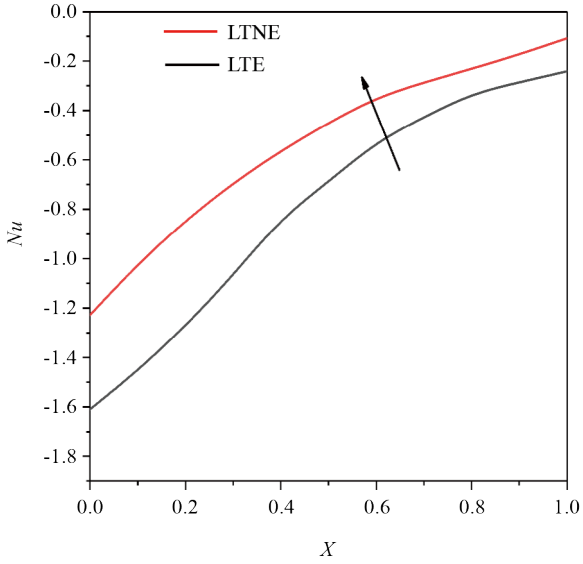


Figure 10. Variation of Nu on LTE and LTNE

For both LTE and LTNE models, the Nu gradually drop throughout the fin length, as seen in Figure 10 and Table 5, suggesting a slow decline in the rate of heat transmission. The LTNE model has greater Nu values improved by 26.19% compared to the LTE model, signaling enhanced heat transfer due to the temperature difference between solid and fluid phases. The difference between LTE and LTNE values is smaller as X increases. This demonstrates that non-equilibrium effects are weaker at the tip and more pronounced close to the fin base.

Table 5. Nusselt number for rectangular fin for LTE and LTNE model when $R = 0.2$, $\chi = 0.3$, $\tau = 1.2$, $Ra = 2$, $Rsa = 2$, $\Omega = 2$, $H = 2$

X	Nu	
	LTE	LTNE
0	−1.60901	−1.22754
0.1	−1.45366	−1.02203
0.2	−1.27309	−0.84567
0.3	−1.06717	−0.69435
0.4	−0.83786	−0.56382
0.5	−0.58895	−0.44976
0.6	−0.33652	−0.34784
0.7	−0.25418	−0.20665
0.8	−0.24866	−0.23146
0.9	−0.19598	−0.17372
1	−0.09129	−0.10846

The observations from the graphs demonstrated that rectangular fin under LTNE model captured the behavior of heat transport more precisely. Thus, ANN has been employed to further investigate the rate of heat transfer in LTNE in order to increase prediction accuracy and optimization.

5. Artificial neural networking

ANNs, which draw inspiration from biological nerve systems and brain structure. Over the past few decades ANN serves as a foundation for a wide range of new techniques and extremely adaptive to complicated problem-solving as they are information processing systems with exceptional learning and generalization capacities [38–43]. Figure 11 shows a schematic representation of the ANN created in this study. The ANN is made up of five neurons in the input layer, sixteen neurons in the hidden layer, and one neuron in the output layer. The output layer uses a linear activation function, but the hidden layer uses a nonlinear activation function (such as sigmoid or tanh). The dataset is split 70 : 15 : 15 into training, validation, and testing sets. The ANN employed in this work as a surrogate model which effectively handles and forecasts large amounts of data obtained by RKF-45 numerical method. Further, the data is used to train the network, guaranteeing precise prediction of the temperature profiles derived from the numerical simulations. ANN showed its peak performance at Epoch 10 with an incredibly low loss value of 3.3498×10^{-6}, signifying great accuracy and low error as depicted in Figure 12. It facilitates quick predictions for new parameter sets and depicts intricate nonlinear relationships.

An ANN efficacy must be evaluated by analyzing the error histogram. The majority of the data points in the histogram are grouped close to the zero-error axis, which shows the errors that were noted during the training, testing, and validation stages. This shows that real values and the model's predictions are fairly similar. Furthermore, Figure 13 which splits the error histogram into 20 bins, emphasizes that the highest accuracy of training is confirmed by the smallest error values. Based on the overall distribution, it appears that the ANN model continues to perform reasonably well in terms of prediction accuracy.

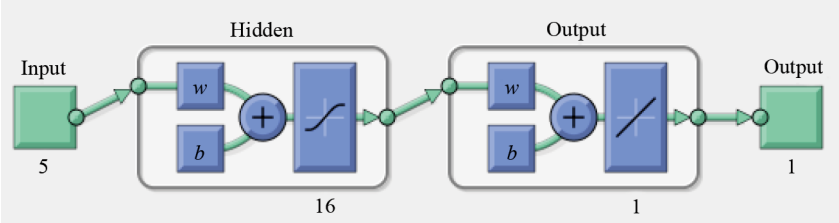


Figure 11. The fundamental structure of the ANN models

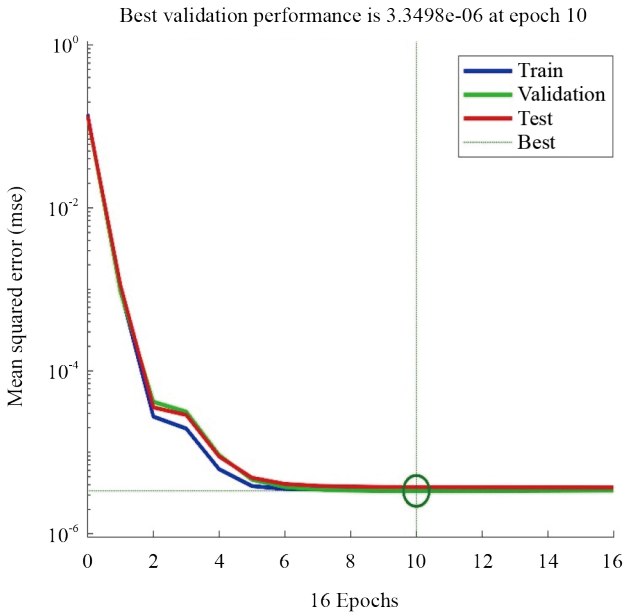


Figure 12. Evaluation of ANN performance

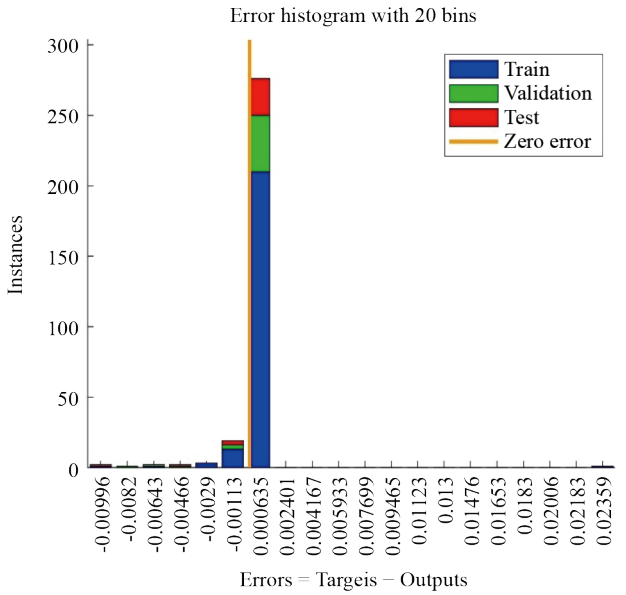


Figure 13. The ANN error histogram

The performance of the ANN regression model during the training, validation, and testing phases is displayed in Figure 14, which also shows the correlation between the expected and actual values. High accuracy is indicated by data points that closely resemble the ideal $y = x$ line in a well-trained model. The model's predictive power is revealed by regression analysis, where the regression coefficient R demonstrates a strong but imperfect correlation between expected and actual values. The model's fit is further indicated by the R value, where higher values signify improved predicting accuracy. The ANN's capacity for generalization is evaluated with the aid of distinct regression plots for each step, guaranteeing dependable performance with less error.

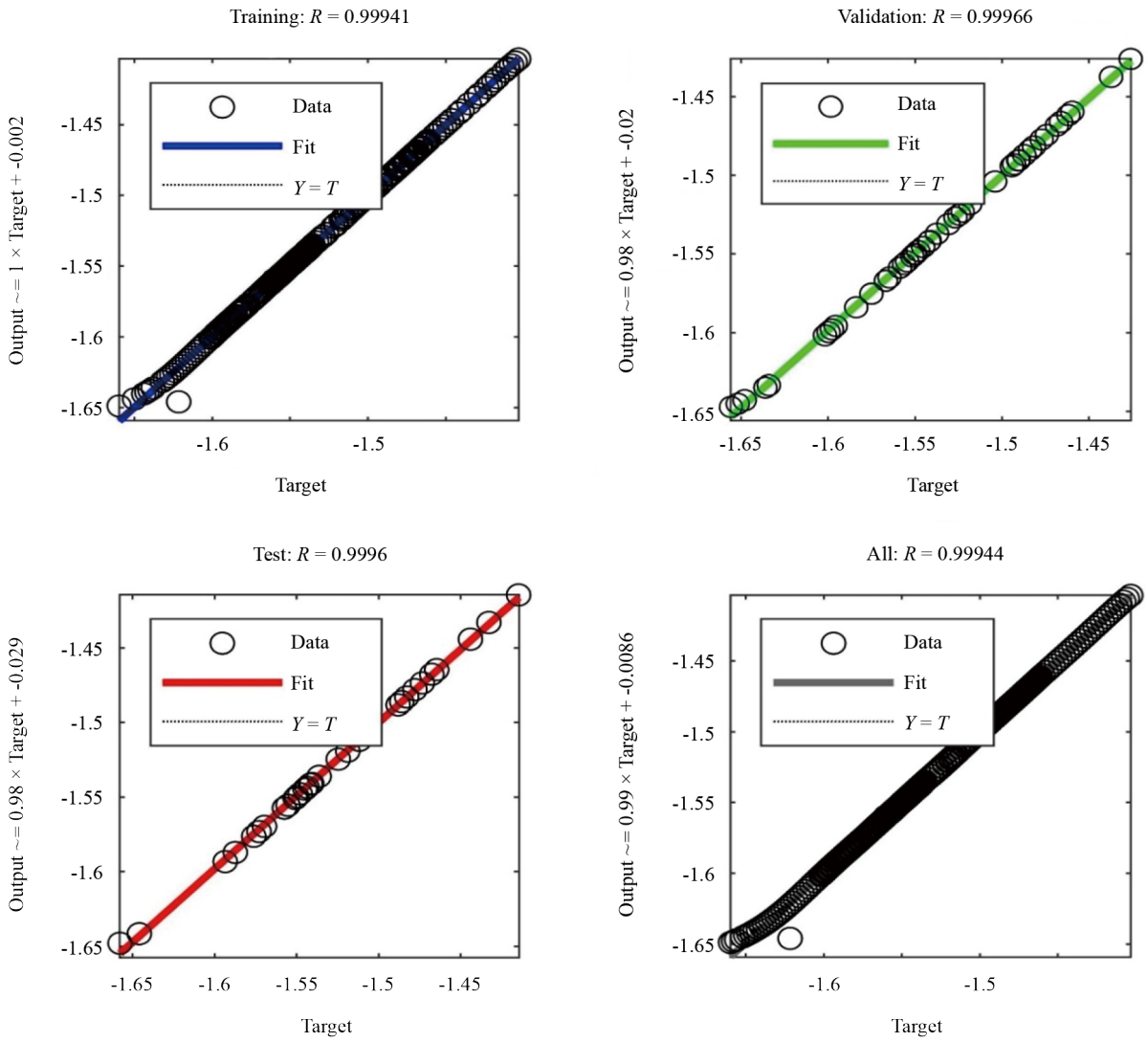


Figure 14. The ANN error histogram

6. Conclusion

The current study compares the LTE and LTNE models for rectangular and triangular profiles in order to provide a thorough examination of the thermal performance of fin systems with variable thermal conductivity. The mathematical method involves nonlinear ODEs for both ternary nanofluid and solid phases, which are reformed into a dimensionless

system by utilizing non-dimensional variables, then solved by employing RKF-45 method. The following conclusions are reached in regard to the findings and discussion:

• The smaller surface area of triangular fins allows them to sustain lower temperatures than rectangular fins.

• LTNE scenarios have greater solid surface temperatures than LTE with the Nusselt number showing 26.19% improvement.

• Higher the concentrations of nanoparticles in nanofluids enhance thermal performance.

• Rise in the magnetic fields reduce convection and promote buoyancy-driven transmission of heat and conduction, which lowers temperatures.

• Increased thermal conductivity reduces temperature fluctuation and promotes even heat distribution.

• An increase in χ improves heat transfer by increasing internal radiation and reducing radiative-conductive resistance.

• The analysis of the ANN model for heat transport in rectangular fins with ternary nanofluid revealed a great predictive performance and a minimal loss of 3.3498×10^{-6}.

• The outcomes are applicable to advanced cooling technologies, electronic thermal management, aerospace heat exchangers, and magnetic microchannel systems where precise thermal control is essential.

Acknowledgments

The authors would like to thank Prince Sultan University, Saudi Arabia, for the technical support through the TAS research lab.

Data availability statement

Data will be available on request.

Conflict of interest

The authors declare no competing financial interest.

References

[1] Harper RR, Brown WB. *Mathematical equations for heat conduction in the fins of air-cooled engines*. Report number: NACA-TR-158, 1923.

[2] Güvenç A, Yüncü H. An experimental investigation on performance of fins on a horizontal base in free convection heat transfer. *Heat and Mass Transfer*. 2001; 37(4): 409–416. Available from: https://doi.org/10.1007/s002310000139.

[3] Chabane F, Moummi N, Benramache S. Experimental study of heat transfer and thermal performance with longitudinal fins of solar air heater. *Journal of Advanced Research*. 2014; 5(2): 183–192. Available from: https://doi.org/10.1016/j.jare.2013.03.001.

[4] Varun Kumar RS, Sowmya G, Jayaprakash MC, Prasannakumara BC, Khan MI, Guedri K, et al. Assessment of thermal distribution through an inclined radiative-convective porous fin of concave profile using generalized residual power series method (GRPSM). *Scientific Reports*. 2022; 12(1): 13275. Available from: https://doi.org/10.1038/s41598-022-15396-z.

[5] Kiwan S, Al-Nimr MA. Using porous fins for heat transfer enhancement. *Journal of Heat Transfer*. 2001; 123(4): 790–795. Available from: https://doi.org/10.1115/1.1371922.

[6] Saedodin S, Sadeghi S. Temperature distribution in long porous fins in natural convection condition. *Middle-East Journal of Scientific Research*. 2013; 13(6): 812–817.

[7] Ahmadpour V, Ahmadi N, Rezazadeh S, Sadeghiazad M. Numerical analysis of thermal performance in a finned cylinder for latent heat thermal system (LHTS) applications. *International Journal of Heat and Technology*. 2013; 31(1): 155–162.

[8] Han Y, Peng X. Thermal performance of a moving fin with temperature-dependent thermal conductivity in convective and radiative environment. *Heliyon*. 2025; 11(3): e42329. Available from: https://doi.org/10.1016/j.heliyon.2025.e42329.

[9] Rostami S, Ahmadi N. In the study of the effects of the pipe design of a heat exchanger on the thermo-fluid characteristics and exergy destruction. *Processes*. 2025; 13(3): 835. Available from: https://doi.org/10.3390/pr13030835.

[10] Ullah I, Ullah S, Ali A, Shah SI, Weera W, Alam MM. Heat transfer analysis from moving convection-radiative triangular porous fin exposed to heat generation. *Case Studies in Thermal Engineering*. 2022; 38: 102177. Available from: https://doi.org/10.1016/j.csite.2022.102177.

[11] Saqib SU, Farooq U, Fatima N, Shih YT, Mir A, Kolsi L. Novel recurrent neural networks for efficient heat transfer analysis in radiative moving porous triangular fin with heat generation. *Case Studies in Thermal Engineering*. 2024; 64: 105516. Available from: https://doi.org/10.1016/j.csite.2024.105516.

[12] Ndlovu PL, Moitsheki RJ. Steady state heat transfer analysis in a rectangular moving porous fin. *Propulsion and Power Research*. 2020; 9(2): 188–196. Available from: https://doi.org/10.1016/j.jppr.2020.03.002.

[13] Adhikari RC, Wood DH, Pahlevani M. An experimental and numerical study of forced convection heat transfer from rectangular fins at low Reynolds numbers. *International Journal of Heat and Mass Transfer*. 2020; 163: 120418. Available from: https://doi.org/10.1016/j.ijheatmasstransfer.2020.120418.

[14] Shadlaghani A, Tavakoli MR, Farzaneh M, Salimpour MR. Optimization of triangular fins with/without longitudinal perforate for thermal performance enhancement. *Journal of Mechanical Science and Technology*. 2016; 30: 1903–1910. Available from: https://doi.org/10.1007/s12206-016-0349-5.

[15] Menni Y, Azzi A. Effect of fin spacing on turbulent heat transfer in a channel with cascaded rectangular-triangular fins. *Journal of New Technology and Materials*. 2017; 7(2): 10–21.

[16] Madhura KR, Babitha, Kalpana G, Makinde OD. Thermal performance of straight porous fin with variable thermal conductivity under magnetic field and radiation effects. *Heat Transfer*. 2020; 49(8): 5002–5019. Available from: https://doi.org/10.1002/htj.21864.

[17] Roy PK, Mallick A, Mondal H, Sibanda P. A modified decomposition solution of triangular moving fin with multiple variable thermal properties. *Arabian Journal for Science and Engineering*. 2018; 43: 1485–1497. Available from: https://doi.org/10.1007/s13369-017-2983-3.

[18] Ananth Subray PV, Hanumagowda BN, Varma SVK, Zidan AM, Kbiri Alaoui M, Raju CSK, et al. Dynamics of heat transfer analysis of convective-radiative fins with variable thermal conductivity and heat generation: differential transformation method. *Mathematics*. 2022; 10(20): 3814. Available from: https://doi.org/10.3390/math10203814.

[19] Chiu CH, Chen CK. A decomposition method for solving the convective longitudinal fins with variable thermal conductivity. *International Journal of Heat and Mass Transfer*. 2002; 45(10): 2067–2075. Available from: https://doi.org/10.1016/S0017-9310(01)00286-1.

[20] Choi SU, Eastman JA. Enhancing thermal conductivity of fluids with nanoparticles. In: *1995 International Mechanical Engineering Congress and Exhibition*. San Francisco, CA, United States: American Society of Mechanical Engineers; 1995. p.99–105.

[21] Jalili B, Aghaee N, Jalili P, Ganji DD. Novel usage of the curved rectangular fin on the heat transfer of a double-pipe heat exchanger with a nanofluid. *Case Studies in Thermal Engineering*. 2022; 35: 102086. Available from: https://doi.org/10.1016/j.csite.2022.102086.

[22] Khan ZH, Khan WA, Elbaz AM, Qasim M, Alharbi SO, Sun L. Natural convection in triangular fin-shaped cavity with partially heated base using nanofluid. *ZAMM-Journal of Applied Mathematics and Mechanics/Zeitschrift für Angewandte Mathematik und Mechanik*. 2021; 101(12): e202000306. Available from: https://doi.org/10.1002/zamm.202000306.

[23] Gireesha BJ, Sowmya G, Khan MI, Öztop HF. Flow of hybrid nanofluid across a permeable longitudinal moving fin along with thermal radiation and natural convection. *Computer Methods and Programs in Biomedicine*. 2020; 185: 105166. Available from: https://doi.org/10.1016/j.cmpb.2019.105166.

[24] Raju CSK, Sajjan K, Yook SJ. Heat transfer characteristics of rectangular/triangular/convex-shaped fins filled with hybrid nanoparticles under dry and wet conditions. *Physics of Fluids*. 2023; 35(11): 112010. Available from: https://doi.org/10.1063/5.0176926.

[25] Manjunatha S, Puneeth V, Gireesha BJ, Chamkha A. Theoretical study of convective heat transfer in ternary nanofluid flowing past a stretching sheet. *Journal of Applied and Computational Mechanics*. 2022; 8(4): 1279–1286.

[26] Ouada M, Kezzar M, Talbi N, Eid MR, Sari MR, Yousef WM, et al. Heat transfer characteristics of moving longitudinal porous fin wetted with ternary (Cu-Al_2O_3-TiO_2) hybrid nanofluid: ADM solution. *The European Physical Journal Plus*. 2023; 138(9): 861. Available from: https://doi.org/10.1140/epjp/s13360-023-04459-3.

[27] Manjunatha S, Kuttan BA, Jayanthi S, Chamkha A, Gireesha BJ. Heat transfer enhancement in the boundary layer flow of hybrid nanofluids due to variable viscosity and natural convection. *Heliyon*. 2019; 5(4): e01469. Available from: https://doi.org/10.1016/j.heliyon.2019.e01469.

[28] Manaswini R, Hanumagowda BN, Tanuja TN, Kavitha L, Abdulrahman A, Punith Gowda RJ, et al. Sensitive analysis of heat transfer enhancement in ternary Casson nanofluid flow between a conical surface and disk. *Modern Physics Letters B*. 2025; 39(7): 2450420. Available from: https://doi.org/10.1142/S0217984924504207.

[29] Tanuja TN, Rehman KU, Kumar GV, Shatanawi W, Varma SVK, Asghar Z. On thermal performance of spine fin in magnetized hybrid fluid rooted with Cu and MoS_4 nanoparticles. *AIP Advances*. 2024; 14(1): 015068. Available from: https://doi.org/10.1063/5.0176878.

[30] Tanuja TN, Manjunatha S, Migdadi HS, Saadeh R, Qazza A, Khan U, et al. Leveraging artificial neural networks approach for thermal conductivity evaluation in porous rectangular wetted fins filled with ternary hybrid nanofluid. *Journal of Radiation Research and Applied Sciences*. 2024; 17(4): 101125. Available from: https://doi.org/10.1016/j.jrras.2024.101125.

[31] Hoseinzadeh S, Moafi A, Shirkhani A, Chamkha AJ. Numerical validation heat transfer of rectangular cross-section porous fins. *Journal of Thermophysics and Heat Transfer*. 2019; 33(3): 698–704. Available from: https://doi.org/10.2514/1.T5583.

[32] Jeng TM, Tzeng SC, Hung YH. An analytical study of local thermal equilibrium in porous heat sinks using fin theory. *International Journal of Heat and Mass Transfer*. 2006; 49(11–12): 1907–1914. Available from: https://doi.org/10.1016/j.ijheatmasstransfer.2005.11.012.

[33] Jaiswal M, Hanumagowda BN, Subray PA, Varma SVK, Khan U, Sarris IE, et al. Thermal scrutinization of a triangular porous fin induced by linear and nonlinear temperature-dependent heat generation and magnetic field effect: the case of Darcy model. *The European Physical Journal Special Topics*. 2024; 233(13): 2265–2279. Available from: https://doi.org/10.1140/epjs/s11734-024-01114-5.

[34] Manaswini R, Manjunatha S, Chamkha AJ, Tanuja TN. A comparative heat transfer analysis of rectangular fin through LTE and LTNE model. *The European Physical Journal Plus*. 2025; 140(8): 787. Available from: https://doi.org/10.1140/epjp/s13360-025-06711-4.

[35] Thimlapura Nagaraju T, Linganna K, Varma SV, Channaiah S, Kumar RSV, Khan U, et al. Thermal analysis of natural convection in rectangular porous fin wetted with CNTs nanoparticles and thermal radiation. *ZAMM-Journal of Applied Mathematics and Mechanics/Zeitschrift für Angewandte Mathematik und Mechanik*. 2024; 104(8): e202300969. Available from: https://doi.org/10.1002/zamm.202300969.

[36] Manjunatha S, Rehman KU, Kumar JS, Varma SVK, Shatanawi W. On thermal non-equilibrium (TNE) model for heat transfer in ternary ferro-nanofluid with rectangular porous fin. *International Journal of Thermofluids*. 2024; 23: 100757. Available from: https://doi.org/10.1016/j.ijft.2024.100757.

[37] Buonomo B, Cascetta F, Manca O, Sheremet M. Heat transfer analysis of rectangular porous fins in local thermal non-equilibrium model. *Applied Thermal Engineering*. 2021; 195: 117237. Available from: https://doi.org/10.1016/j.applthermaleng.2021.117237.

[38] Bahrammirzaee A. A comparative survey of artificial intelligence applications in finance: artificial neural networks, expert system and hybrid intelligent systems. *Neural Computing and Applications*. 2010; 19(8): 1165–1195. Available from: https://doi.org/10.1007/s00521-010-0362-z.

[39] Khedher NB, Ijaz N, Dhahbi S, Barghout K, Abu-Libdeh N, Zeeshan A. Thermal dynamics assessment for multi-phase flow analysis with motile cilia and electric double layer effects: application of Levenberg-Marquardt backpropagation NNs. *Case Studies in Thermal Engineering*. 2024; 57: 104332. Available from: https://doi.org/10.1016/j.csite.2024.104332.

[40] Eiman, Shah K, Sarwar M, Abdeljawad T. Study of fractional order epidemic compartmental model by using artificial deep neural networks. *Neural Networks*. 2025; 192: 107944. Available from: https://doi.org/10.1016/j.neunet.2025.107944.

[41] Manjunatha S, Manaswini R, Ioan PM, Tanuja TN. Flow and heat transfer of penta-hybrid nanofluid at stagnation point over a stretching/shrinking sheet. *Thermal Science and Engineering Progress*. 2025; 64: 103797. Available from: https://doi.org/10.1016/j.tsep.2025.103797.

[42] Ran J, Zhou Y, Abdeljawad T, Pu H. Discrete fractional neural networks within the framework of octonions: a preliminary exploration. *Journal of Computational Science*. 2025; 87: 102586. Available from: https://doi.org/10.1016/j.jocs.2025.102586.

[43] Ibrahim IS, Baleanu D, Yousif MA, Mohammed PO, Abdeljawad T. Integrating Bessel-type summability and artificial neural networks for sequence classification. *Modeling Earth Systems and Environment*. 2026; 12(1): 47. Available from: https://doi.org/10.1007/s40808-025-02683-7.